Prediction of Current-dependent Motor Torque Characteristics Using Deep Learning for Topology Optimization

Taiga Aoyagi[1], Yoshitsugu Otomo[1], Hajime Igarashi[1], Hidenori Sasaki[2], Yuki Hidaka[2], and Hideaki Arita[2]
[1]Graduate School of Information Science and Technology, Hokkaido University, Sapporo 060-0814, Japan
[2]Advanced Technology Research and Development Center, Mitsubishi Electric Corporation, Amagasaki 661-8661, Japan

In this study, we propose a fast topology optimization method based on a deep neural network (DNN) that predicts the current-dependent motor torque characteristics using its cross-sectional image. The trained DNN is shown to provide the current condition that provides the maximum torque under the assumed motor control method. The proposed method helps perform topology optimization with a reduced number of field computations while maintaining a high search capability.

***Index Terms*—Convolutional neural network (CNNs), deep learning (DL), permanent magnet motor, topology optimization.**

I. Introduction

SINCE RECENTLY, it is being expected that the zero-emission vehicles rapidly spread throughout the world. Accordingly, the development of high-performance electrical motors for these vehicles has become indispensable. Topology optimization (TO) is proven to be effective especially for the initial design stages [1], [2]. Moreover, it does not require the design parameters to be set. The TO method in which the machine structure is represented by the Gaussian basis functions is shown to be effective for motor optimization [3]. In this method, global search is performed using a population-based method, such as genetic algorithm or CMAES. This approach inevitably involves repeated field computations. To reduce the computing cost, a trained convolutional neural network (CNN) is adopted for screening the individuals; only those individuals that are given a high score by the CNN are evaluated using finite element method (FEM) [4]. The trained CNN predicts the torque characteristics from the motor cross-sectional image. This method is proven to reduce the computing cost of TO without compromising the search capability. However, the current amplitude and phase are assumed constant in this method even though they vary according to the motor control. It has been shown that the d and q axis inductances, which are assumed to be constants, can be predicted using CNN from the cross-sectional image of an IPM motor [5]. This method allows us to find the current condition that maximizes the torque. However, because the d and q axis inductances actually depend on the current conditions, this method would be inaccurate in cases where such dependence is significant.

In this paper, we propose a fast TO method based on the CNN which predicts the current-dependent motor torque characteristics, which are represented by a curvilinear surface, using its cross-sectional image. We can obtain the maximum torque condition from this surface under a given motor control condition such as MTPA (maximum torque per ampere), and MTPV (maximum torque er voltage). To verify the effectiveness of the present TO, we optimized the rotor shape of PM motors with I-shaped and V-shaped magnets so that the average torque is maximized while the torque ripple is suppressed as small as possible.

II. PROPOSED METHOD

A. Topology optimization method

The material distribution in the design region of a permanent magnet rotor is determined from the output of a Normalized Gaussian network (NGnet) [3] which is given by

$$f(\boldsymbol{x}) = \sum_{i=1}^{N} w_i b_i(\boldsymbol{x}) \tag{1}$$

$$b_i(\boldsymbol{x}) = G_i(\boldsymbol{x}) / \sum_{k=1}^{N} G_k(\boldsymbol{x}) \tag{2}$$

where, $\boldsymbol{x}$, $G_k(\boldsymbol{x})$, and w_i indicate the position vector, Gaussian basis function, and weighted coefficients, respectively. The material attribute A_e of element e in the design region is determined such that $A_e = \mathrm{iron}(\mathrm{f} >= 0)$, $A_e = \mathrm{air}(\mathrm{f} < 0)$. In the present TO, the weighting coefficient $\boldsymbol{w}$ is determined using the real-coded genetic algorithm named AREX+JGG [6] to minimize the cost function.

B. Prediction of torque characteristics using a CNN

The optimization models are shown in Fig. 1 and the specifications of these models are summarized in Table 1. The

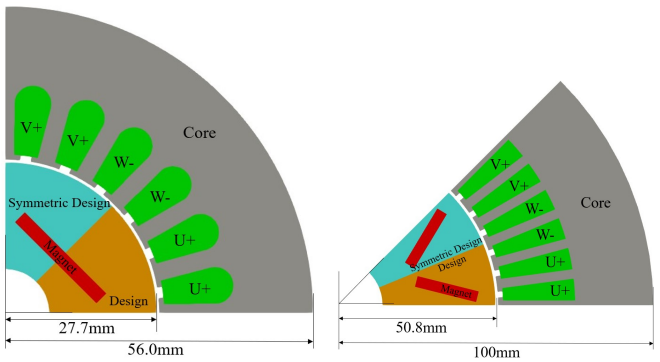

Fig. 1. Optimization models. (a) I-shaped magnet, four poles, 24 slots. (b) V-shaped magnet, eight poles, 48 slots.

TABLE I.
EQUIPMENT SETTINGS FOR THE OPTIMIZATION MODELS

Property	Unit	I-shaped model	V-shaped model
Coil turns		30	20
Core material		50JN400	50JN400
Coil resistance	Ω	1	1
Thickness	mm	100	100
Rotating speed	rpm	1000	1000
Driving frequency	Hz	100/3	200/3
Magnetization of magnet	T	0.8	0.8

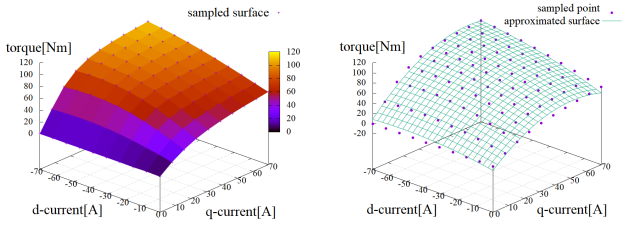

(a) (b)

Fig. 2. Torque distribution on dq current space. (a): Sampling points and smoothed surface. (b): Sampling points and approximated surface.

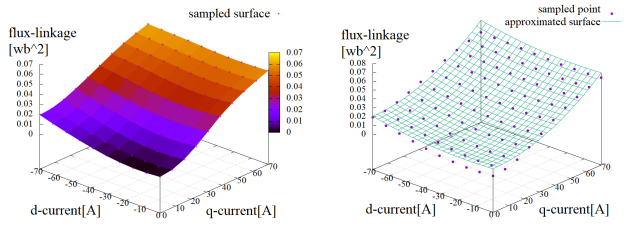

(a) (b)

Fig. 3. Squared flux linkage distribution on dq current space. (a): Sampling points and smoothed surface. (b): Sampling points and approximated surface.

typical torque surface of the IPM motor of interest is shown in Fig. 2(a). We expressed the torque surface as a quadratic polynomial given by:

$$T(i_d, i_q) = \beta_0 i_d^2 + \beta_1 i_q^2 + \beta_2 i_d i_q + \beta_3 i_d + \beta_4 i_q + \beta_5 \quad (3)$$

where, i_d and i_q represent the d and q-axis currents, respectively. As shown in Fig. 2(b), the current characteristics are sampled at 100 points on a grid in the dq-axis current space, and the parameters are determined by the least-squares method. The parameters from β_0 to β_5 are predicted by CNN from the input motor cross-sectional image. Once these parameters are obtained, the currents that maximize the torque for the MTPA control can be estimated. To determine the currents under the MTPV control, we need to evaluate the induced voltage from the magnetic flux that interlinks with the coils. We considered the squared flux linkage Ψ^2, which can be represented by a quadratic polynomial as follows:

$$\Psi^2(i_d, i_q) = \gamma_0 i_d^2 + \gamma_1 i_q^2 + \gamma_2 i_d + \gamma_3 \quad (4)$$

The distribution of Ψ^2 for a typical IPM motor is shown in Fig. 3(a). The least-square interpolation is shown in Fig. 3(b). The parameters from γ_0 to γ_3 are predicted by CNN as well as $\beta_i (i = 0, \cdots, 5)$. It is remarked that the order of

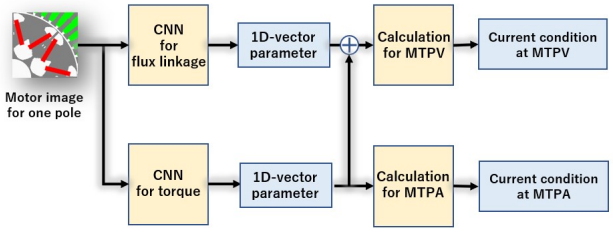

Fig. 4. Flow diagram for estimating the optimal current condition.

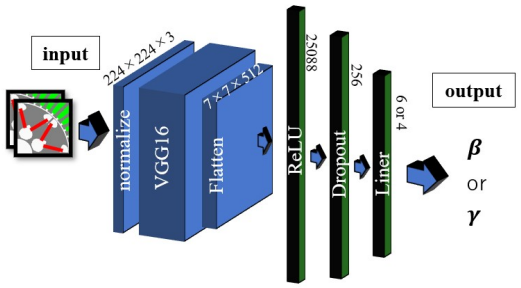

Fig. 5. CNN flow diagram for estimating $\boldsymbol{\beta}$ and $\boldsymbol{\gamma}$.

polynomial for the interpolation would be higher for a larger current value to consider the effect of deep saturation, whereas interpolation (4) appears to be sufficiently accurate for current of up to 70 A, which is assumed to be the maximum current in our optimization. As shown in Fig. 4, we constructed two types of CNNs: one to estimate the flux linkage parameters $\gamma_i (i = 0, \cdots, 3)$ and the other to estimate the torque parameters $\beta_i (i = 0, \cdots, 5)$.

To predict these parameters, we utilized a CNN that was constructed using VGG16 [7], as shown in Fig. 5. Further, we trained it using Image-Net before training it using the motor image data. We generated IPM motors with different flux barriers by performing a preliminary topology optimization to obtain 12,900 samples for each of the I-shaped and V-shaped models. These data samples were further divided into 9,030 and 3,870, which were used for training and testing, respectively. Moreover, we stored the corresponding parameters $\boldsymbol{\beta}(= \{\beta_0, \cdots, \beta_5\})$ and $\boldsymbol{\gamma}(= \{\gamma_0, \cdots, \gamma_3\})$ to train CNN.

III. NUMERICAL RESULTS

First, we considered the prediction accuracy of CNNs. Fig. 6 shows the correlation between the observed and predicted values of the selected polynomial coefficients for I-shaped and V-shaped models. The correlation coefficient r, mean absolute error (MAE) and root mean square error (RMSE) for all the coefficients are summarized in Table 2. Although the overall prediction accuracy appears to be sufficient for the optimization, the r values for β_0 and γ_0 are smaller than 0.9. We observed that these correlations are relatively weaker due to the randomly distributed iron cores of the motors. Because this finding appears in the first generation of the genetic algorithm used for the optimization it would give a limited effect on the optimization. We performed TO using the trained CNN for both models. The optimization problem is defined by

$$F(\boldsymbol{w}) = -1.2\frac{T_{\text{avg}}(\boldsymbol{w})}{T_{\text{avg}}^{\text{ref}}} + 0.1\frac{T_{\text{rip}}(\boldsymbol{w})}{T_{\text{rip}}^{\text{ref}}} \to \min \quad (5)$$

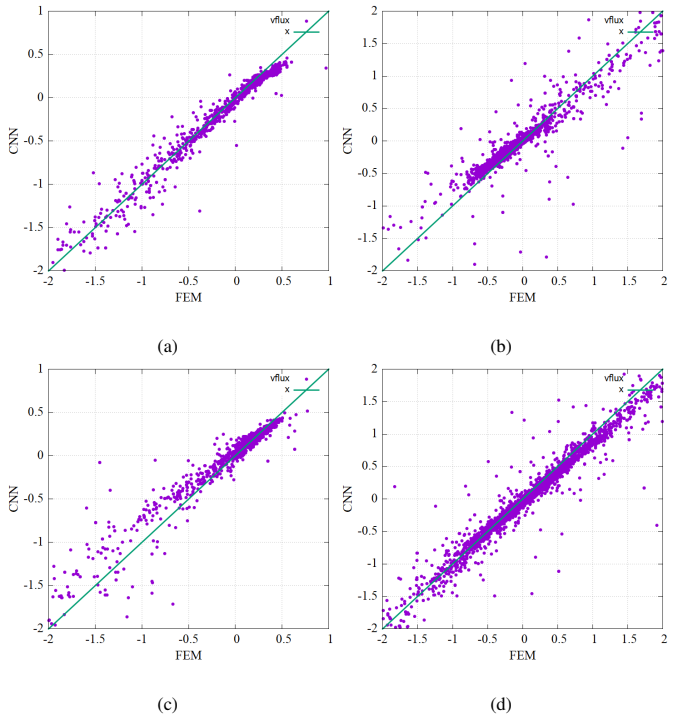

Fig. 6. Correlation of coefficients obtained from FEM and CNN for each model and parameters. (a) V-shaped model γ_3 r = 0.984. (b) V-shaped model β_2 r = 0.945. (c) I-shaped model γ_1 r = 0.985. (d) I-shaped model β_0 r = 0.956.

TABLE II.
STATISTICS OF ESTIMATION ERROR

parameter	Model	r	MAE	RMSE
γ_0	V-shaped model	0.964	0.134	0.289
γ_1	V-shaped model	0.971	0.128	0.292
γ_2	V-shaped model	0.974	0.111	0.264
γ_3	V-shaped model	0.984	0.076	0.206
β_0	V-shaped model	0.884	0.142	0.450
β_1	V-shaped model	0.978	0.0864	0.222
β_2	V-shaped model	0.945	0.0972	0.312
β_3	V-shaped model	0.856	0.135	0.489
β_4	V-shaped model	0.982	0.0847	0.213
β_5	V-shaped model	0.900	0.171	0.466
γ_0	I-shaped model	0.848	0.144	0.765
γ_1	I-shaped model	0.985	0.0606	0.207
γ_2	I-shaped model	0.930	0.109	0.611
γ_3	I-shaped model	0.983	0.0643	0.219
β_0	I-shaped model	0.956	0.114	0.315
β_1	I-shaped model	0.984	0.0949	0.190
β_2	I-shaped model	0.983	0.0954	0.197
β_3	I-shaped model	0.971	0.100	0.260
β_4	I-shaped model	0.985	0.0893	0.190
β_5	I-shaped model	0.980	0.101	0.216

where, $T_{\rm avg}(\boldsymbol{w})$ and $T_{\rm rip}(\boldsymbol{w})$ denote the average torque and torque ripple, respectively, and the quantities with the index " ref " represent the values for the reference motor. Moreover, $\boldsymbol{w}$ denotes the vector composed of the weighting coefficients to the Gaussian basis functions used for the topology optimization [3]. We then used genetic algorithm to find $\boldsymbol{w}$ that minimized F. We performed three optimizations: the conventional method, where the current condition was not altered [3], and the optimizations under the MTPA and MTPV controls. The

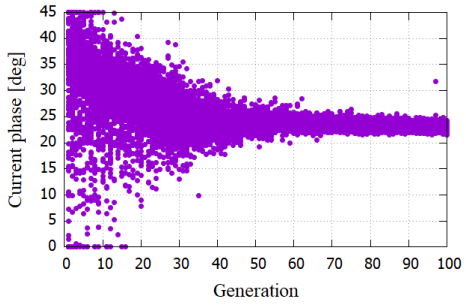

Fig. 7. Estimated current phase angle during optimization in MTPA for V-shaped magnet model. The final state is $(i_d, i_q) : (-17.8, 41.3)$A.

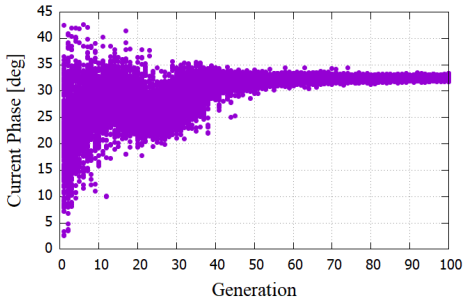

Fig. 8. Estimated current phase angle during optimization in MTPA for I-shaped magnet model. The final state is $(i_d, i_q) : (-19.1, 29.3)$A.

current amplitude I and phase angle β in the conventional method were set to $(i_d, i_q) : (-15.4, 42.3)$A for the V-shaped model and $(i_d, i_q) : (-17.5, 30.3)$A for the D-shaped model. During the optimization under the MTPA control, the phase angles β computed by CNN for the individuals changed for both models as generations proceeded, as plotted in Figs. 7 and 8. In the initial populations, the β values exhibited wide distribution, whereas, they converged to a value between 20° and 25° for MTPA, and to a value between 31° and 34° for MPTA. Figs. 9 and 10 show the evolution of the $d-$ and $q-$ current components evaluated by CNN during the optimization of both models under the MTPV control. We maintained constant (i_d, i_q) for the five first generations. In Figs. 9 and 10, it can be seen that the current state converges to approximately $(i_d, i_q) : (-35, 51)$A for the V-shaped model and $(i_d, i_q) : (-19, 38)$A for the I-shaped model. The assumed current states in the conventional method are shown in Figs. 10 and 11 for the reference. Figs. 11 and 12 show the optimized shapes obtained by the conventional method [3], in which the current conditions are constant, and those obtained by the proposed method, respectively. Comparing the results in (a) with that in (b), although the average torques are approximately equal, the torque ripple is improved by the proposed method considering MTPA. Moreover, because the final current states of MTPA happen to be in the vicinity of those assumed in the conventional method, there is no significant difference in shapes depicted in Fig. 12(a) and (b). In contrast, the results obtained assuming the MTPV control, as shown in Fig. 12(c), are different from those in (a) and (b). Furthermore, because the converged current amplitude resulted from the MTPV control is greater than the that obtained by conventional approach,

$T_{\rm avg}$ obtained using MTPV is greater than that attained using the other two cases. Therefore, it can be said that the motor obtained under the MTPV control is reluctance-torque oriented.

For the individuals generated in the optimization process, searching for the optimal current conditions by changing (i_d, i_q) using FEM would require a huge computational cost [8]. In comparison, the computational cost required by the proposed method is approximately 80% lower than that in the case of conventional method based on the search for the optimal current condition on the grid of 10×10 nodes in the i_d - i_q space. When using CPU: Intel(R) Xeon(R) E5- 2637v4×2 (Clock: 3.5 GHz, cores: 4, threads: 16, 64 GB RAM) in our computing environment, the computing times per generation observed for the conventional and the proposed methods were 1302 s and 288 s, respectively. In addition to this computing time, the proposed method requires additional computing time to construct CNN for optimization, that is, the preliminary optimization for constructing training data and training the CNN. It took 376 minutes to build the training data and 695 minutes to train the CNN. Even after considering these additional time durations, the proposed method works 30% faster than the conventional method. Moreover, once the CNN is trained, it works swiftly for the optimization problems with different weighting coefficients in the cost function (5) and with different constraints.

IV. Conclusion

In this paper, we have proposed topology optimization based on the deep neural network that predicts the torque and induced voltage dependent on the current amplitude and phase. Using the proposed method, we can find the optimal shape of the rotor and simultaneously the optimal current condition under MTPA and MTPV. The proposed method can also apply to the flux weakening control. The proposed method reduces the computing cost by 80% in comparison with the conventional method with search for optimal current condition.

References

[1] A. N. A. Hermann, N. Mijatovic and M. L. Henriksen, "Topology optimisation of PMSM rotor for pump application," *ICEM*, 2016, pp. 2119-2125.

[2] T. Labbé, B. Dehez, M. Markovic and Y. Perriard, "Torque-to-weight ratio maximization in PMSM using topology optimization," *The XIX International Conference on Electrical Machines - ICEM 2010*, 2010, pp. 1-5

[3] T. Sato, K. Watanabe, and H. Igarashi, "Multimaterial topology optimization of electric machines nased on normalized Gaussian network," *IEEE Trans. Magn.,* vol 51, no. 3, Mar. 2015, Art. no. 7202604.

[4] H. Sasaki and H. Igarashi, "Topology optimization accelerated by deep learning," *IEEE Trans. Magn.,* vol. 55, no 6, Jun. 2019, Art. no 740130

[5] H. Sato and H. Igarashi, "Deep-Learning-based Surrogate Model for Fast Multi-material Topology Optimization of IPM Motor," COMPEL, 2021, Vol.ahead-of-print, No.ahead-of-print.

[6] A.Komori, "Efficient Numerical Optimization Algorithm Based on New Real-Coded Genetic Algorithm, AREX + JGG, and Application to the Inverse Problem in Systems Biology," Applied Mathematics. 03. pp. 1463-1470.

[7] K. Simonyan and A. Zisserman, "Very Deep Convolutional Networks for Large-Scale Image Recognition, " Sep. 2014, arXiv 1409.1556.

[8] X.Chen, J.Wang, B.Sen, P. Lazari and T.Sun, "A High-Fidelity and Computationally Efficient Model for Interior Permanent-Magnet Machines Considering the Magnetic Saturation, Spatial Harmonics, and Iron Loss Effect, " *IEEE Trans. Ind. Electron.,* vol. 62, no. 7, July 2015. pp.4044-4055.

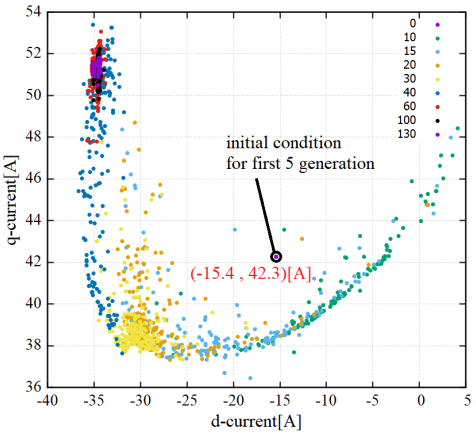

Fig. 9. Evolution of $d-$ and $q-$ current components for I-shaped motor under MTPV control. The number represent the generation of genetic algorithm (same in Fig.10).

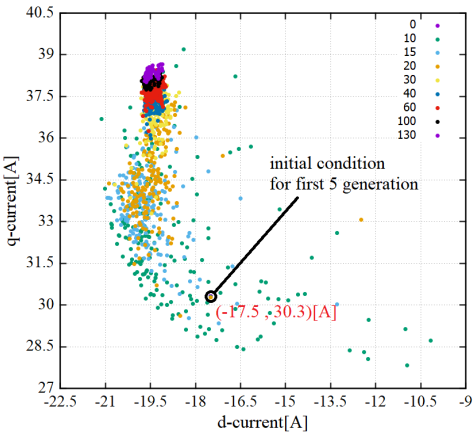

Fig. 10. Evolution of $d-$ and $q-$ current components for V-shaped motor under MTPV control.

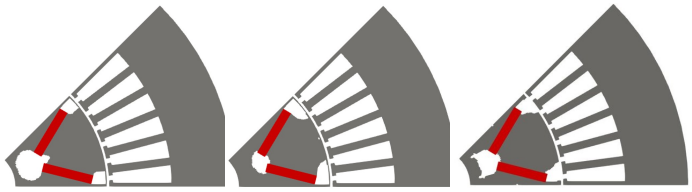

(a) Conventional method (b) Proposed method MTPA (c) Proposed method MTPV

Fig. 11. Optimized V-shaped magnet model shapes.
(a):$T_{\rm avg}$: 33.89(N/m), $T_{\rm rip}$: 0.520 at (i_d, i_q) : $(-15.4, 42.3)$A.
(b):$T_{\rm avg}$: 33.91(N/m), $T_{\rm rip}$: 0.119 at (i_d, i_q) : $(-17.8, 41.3)$A.
(c):$T_{\rm avg}$: 49.30(N/m), $T_{\rm rip}$: 0.890 at (i_d, i_q) : $(-34.6, 51.5)$A.

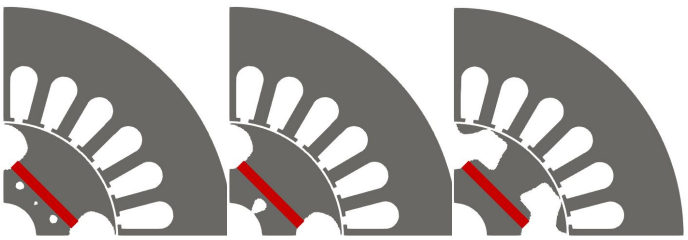

(a) Conventional method (b) Proposed method MTPA (c) Proposed method MTPV

Fig. 12. Optimized I-shaped magnet model shapes.
(a):$T_{\rm avg}$: 14.52(N/m), $T_{\rm rip}$: 0.230 at (i_d, i_q) : $(-17.5, 30.3)$A.
(b):$T_{\rm avg}$: 14.93(N/m), $T_{\rm rip}$: 0.219 at (i_d, i_q) : $(-19.1, 29.3)$A.
(c):$T_{\rm avg}$: 25.33(N/m), $T_{\rm rip}$: 0.471 at (i_d, i_q) : $(-19.4, 38.3)$A.